https://doi.org/10.3311/PPch.17619

Periodica Polytechnica Chemical Engineering, 65(3), pp. 389–399, 2021

Simultaneous Removal of Cu^{2+}, Zn^{2+} and Cd^{2+} from Aqueous Solutions by Alkali Activated Slag

Milena Tadić[1*], Miljan Bigović[2], Dijana Djurović[3], Martina Jakić[1], Irena Nikolić[1]

[1] Faculty of Metallurgy and Technology, University of Montenegro, DžordžaVašingtona bb, 81000 Podgorica, Montenegro
[2] Faculty of Natural Sciences, University of Montenegro, DžordžaVašingtona bb, 81000 Podgorica, Montenegro
[3] Institute of Public Health of Montenegro, DžonaDžeksona bb, 81000 Podgorica, Montenegro
[*] Corresponding author, e-mail: milenak@ucg.ac.me

Received: 02 December 2020, Accepted: 15 February 2021, Published online: 20 May 2021

Abstract

Electric Arc Furnace (EAF) slag containing larnite, gehlenite, wuestite, montcellite and calcite as the main crystal phases was alkali activated using the alkali activator prepared by the mixing of two solutions, sodium silicate and NaOH. Alkali Activated (AA) slag based on EAF slag is used as an adsorbent for Cu^{2+},Cd^{2+} and Zn^{2+} from aquatic solutions performing the *batch* adsorption test at the range temperature between 20 and 45 °C. AA slag sample is characterized by XRPD, FTIR and SEM/EDS analysis and the results indicate crystalline-amorphous structure of AA slag that contains Calcium Aluminate Silicate Hydrate (C-A-S-H) phase. Concentration of Cu^{2+}, Cd^{2+} and Zn^{2+} in aqueous solution was determined using Inductively Coupled Plasma Optical Emission Spectrometry (ICP-OES). The results obtained indicate that, in a multicomponent system of three dissolved ions, AA slag shows highest affinity towards the Cu^{2+}. The order of the metal ion adsorption onto AA slag was: Cu^{2+}, Cd^{2+} and Zn^{2+}. The highest adsorption of Cu^{2+} is attributed to the highest electronegativity and lowest hydrated ionic radii of cation in comparison to Cd^{2+} and Zn^{2+}. Pseudo-first-order and pseudo-second-order kinetics models, Langmuir and Freundlich isotherm models were applied in order to investigate the adsorption process. The results have shown that data better fitted the pseudo-second kinetic and Langmuir isotherm models The investigation of mechanism of adsorption indicate that both film diffusion and intra-particle diffusion have occurred during the adsorption process. The thermodynamics parameters of adsorption process indicate the spontaneous and endothermic character of heavy metals adsorption on the AA slag.

Keywords

copper, cadmium, zinc, adsorption, Alkali Activated (AA) slag

1 Introduction

Different industrial activities (mining, metallurgical and agricultural sectors) inevitably lead to the generation of wastewaters leaden with the heavy metals [1]. Discharges of industrial effluents into natural recipient without any pre-treatment, presents a potential risk for human health due to the natural waters and soil pollutions.

Cu and Zn are essential for living organisms, but when their content exceeds some limits in water these metals show a toxic effect leading to the serious health problems like brain and kidney damage, chronic anemia, stomach and intestine irritation, fatigue, vomiting, renal damage, and cramps [2]. On the other hand, Cd exhibits a highly toxic effect on a human health even in a small concentration and its health hazard is reflecting in cancerous and mutagenic diseases [2].

Adsorption has been proposed as a highly efficient and cost efficient method for removal of heavy metals from aqueous solution. Different sorbents have been proposed for this purpose, but a special attention was paid to the use of agricultural waste [3] and industrial by-products [4] as an low-cost sorbent for heavy metals removal from wastewaters treatment. The pristine fly ash, the by-product of coal combustion in a coal fired power stations can be used as an effective adsorbent for heavy metal removal from wastewaters [5]. Red mud, bauxite ore processing waste [6], iron making slag [7] and steel making slag [8] were also considered as promising low-cost adsorbents for wastewaters treatment.

The sorption properties of industrial by-products can be improved by their modification by different means. In this sense, microwave-assisted alkali modification of

Cite this article as: Tadić, M., Bigović, M., Djurović, D., Jakić, M., Nikolić, I. "Simultaneous Removal of Cu^{2+}, Zn^{2+} and Cd^{2+} from Aqueous Solutions by Alkali Activated Slag", Periodica Polytechnica Chemical Engineering, 65(3), pp. 389–399, 2021. https://doi.org/10.3311/PPch.17619

fly ash [9] mechanical modification [10] and modification with functionalized mesoporous silica [11] have been proposed. Due to the high content of SiO_2 and Al_2O_3, fly ash has also been proposed as a precursor for a synthesis of zeolite-type adsorbent material for heavy metal removal from wastewaters [12]. The efficiency of heavy metals removal from wastewaters using a red mud can be enhanced by its seawater neutralization [13], iron oxide activation [14] and acid activation [15].

Calcium Silicate Hydrate (C-S-H) has also been proposed as an efficient adsorbent for heavy metals removal [16]. Al substituted C-S-H, *i.e.* Calcium Aluminate Silicate Hydrate (C-A-S-H) can also be used for this purpose [17]. Since amorphous C-A-S-H is recognized as a reaction product of slag alkali activation, this study highlights the potential use of Alkali Activated slag (AA slag) for heavy metals removal from wastewaters. Slag alkali activation implies the chemical reaction between powdered slag and alkali activator (mainly sodium silicate solution) yielding the formation of reaction product - amorphous C-A-S-H gel. The final structure of Alkali Activated slag is heterogeneous and contains unreacted slag grains bounded in a reaction product of slag alkali activation [18].

AA slag was widely investigated in a pass decade as a potential replacement for a cement binder and eventual application in a civil engineering. Mainly Granulated Blast Furnace Slag (GBFS), the by-product of iron production was used as raw materials for the synthesis of AA slag, due to the high content of amorphous phase which is essential for formation of amorphous C-A-S-H gel. However, an important shift towards the use of steel making slag (EAF slag in this research) was also observed [19]. EAF slag is characterized by the significantly higher crystallinity in comparison to GBFS which makes it difficult for a formation of amorphous C-A-S-H gel during the alkali activation process. Therefore, in this research EAF slag was utilized for a synthesis of AA slag which was used as an adsorbent for simultaneous Cu^{2+}, Zn^{2+} and Cd^{2+} from aqueous solutions containing all three metal species. The efficiency of application of AA slag based on EAF slag as an adsorbent was studied by the evaluation contact time and temperature of adsorption process. Isotherm, kinetics, diffusion mechanism and thermodynamic models were evaluated, as well.

2 Materials and methods

Alkali Activated slag (AA slag) used in this research as a sorbent was prepared by using steel making, Electric Arc Furnace slag (EAF slag) supplied from the Still Mill in Montenegro which chemical composition is given in Table 1. The main crystal phases present in EAF slag sample were larnite, wüstite, gehlenite and montcellite, while calcite phase was also present in smaller quantity (Fig. 1).

AA slag was prepared by mixing powdered EAF slag with alkali solution in a solid to liquid mass ratio of 4. The mixture of Na_2SiO_3 solution (commercial water glass: Na_2O = 8.5 %, SiO_2 = 28.5 %, density of 1.39 kg m^{-3}) and the solution of 10 M NaOH mixed in mass ratio of 1:2 was used as an alkali solution. The paste obtained after mixing of EAF slag with alkali solution was casted into plastic mould, sealed with lead and cured in the oven at 65 °C for the period of 48 h. After that the hardened monolith sample was removed from mould and left to stay for 28 days at ambient temperature before being powdered to a particle size bellow 65 μm. Subsequently, the sorbent was washed with deionized water until the pH of the water was kept at value 7±0.5 and then dried at 105 °C.

AA slag sample was characterized by X-Ray Powder Diffraction (XRPD) technique, Fourier Transform Infrared (FT–IR) spectroscopy and Scanning Electron Microscopy (SEM). The XRPD data were collected on a Rigaku

Table 1 Chemical composition (in %) of EAFS

Component	%
CaO	46.5
FeO	23.5
SiO_2	12.2
Al_2O_3	7.2
MgO	6.5
MnO	1.3
TiO_2	1.06
Fe_2O_3	0.9
Cr_2O_3	0.8
L,O:I*	2.4

*Loss on ignition

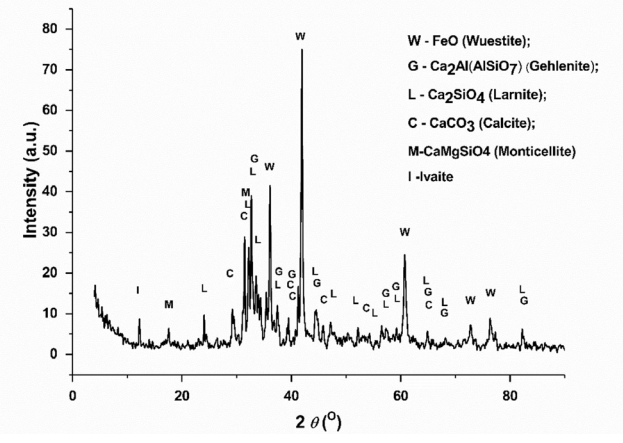

Fig. 1 X-ray difractogram of EAF slag

RINT-TTRIII diffractometer, with Cu-Kα radiation of λ = 1.5406 Å at room temperature in the 2θ range of 10–70° with a scanning step of 0.02° and scan speed of 5 s per step.

Fourier Transform Infrared (FT–IR) spectra were recorded using the Thermo Scientific™ Nicolet™ i S™ 10 FT–IR Spectrometer equipped with Attenuated Total Reflectance (ATR) accessory. Microstructural investigations were carried out using the FEI 235 DB focused ion beam system, equipped with the EDAX Energy Dispersive Spectrometer (EDS). The SEM images were recorded with various electron detectors, including the secondary electron detector.

The adsorption tests were carried out in a batch conditions for a period of 35 min at adsorbent dosage of 0.4 g l^{-1} and pH of 5 at the temperatures of 20, 35 and 45 °C. The test related to the investigations of kinetic, diffusion mechanism and thermodynamic were carried out at constant initial metals concentration of 100 ppm while adsorption isotherm tests were carried out in the concentration range of 20–120 ppm. Multicomponent solution containing all three metal ions (Cu^{2+}, Zn^{2+} and Cd^{2+}) was prepared from analytical grade chemicals, $CuSO_4 \times 5H_2O$, $ZnSO_4 \times 5H_2O$ and $CdSO_4 \times 5H_2O$ in deionized water. An aliquot of the suspension was taken at certain intervals of time, filtered and tested for the concentrations of metal ions using Inductively Coupled Plasma Optical Emission Spectrometry (ICP-OES).

Metals Removal Efficiency (RE) was calculated by Eq. (1):

$$\mathrm{RE} = \frac{C_0 - C_t}{C_0} \times 100\ \%, \tag{1}$$

where C_0 and C_t are the initial and final concentrations of metal ions in solution.

The amount of metals uptake by adsorbents *i.e.* adsorption capacity q_t at any given time t was determined by Eq. (2):

$$q_t = \frac{(C_0 - C_t)}{m} \times V, \tag{2}$$

where V is the volume of Cu^{2+} ions solution, and m is the dry mass of adsorbent.

3 Results and discussion

3.1 Sorbent characterization

The result of XRPD analysis has shown that AA slag sample was crystalline-amorphous. The percentage of crystalline and amorphous phase in the AA slag sample, calculated using JADE software, was 58.8 % and 41.2 %, respectively. X-Ray Powder Diffraction pattern of AA slag sample has shown the presence of some undissolved ingredients larnite, gehlenite, wuestite, montcellite and calcite remained from unreacted EAF slag (Fig. 2 (a)).

FTIR spectra of AA slag sample (Fig. 2 (b)) exhibits two bands that comprise the C-A-S-H gel. One at 873 cm^{-1} attributed to Si–OH bending and second one at 967 cm^{-1} ascribed to Si–O stretching vibrations in the SiO_4 tetrahedra [20, 21]. Band at 1640 cm^{-1} is ascribed to H-OH bending of hydroxyl groups and low intensity broad band between 3000 and 3700 cm^{-1} (inset graph) is attributed to the OH bending vibrations in water molecules. The bands attribute to O-C-O bonds in $(CO_3)^{2-}$ (at 709 and 1413 cm^{-1}) were also observed. These two bands correspond to the $CaCO_3$.

Microstructure of AA slag is heterogenous as shown in microphotograph in Fig. 3 It is evident that AA slag sample consists of unreacted slag grains bounded in a reaction product of slag alkali activation (C-A-S-H gel). This is also indicated by EDS composite maps of elemental distribution. It is evident that the presence of Si rich phase around the slag grain can been related to the existance of C-A-S-H gel [22]. Moreover, the presence of Cr was also observed in C-A-S-H gel. The presence of Cr in C-A-S-H gel can

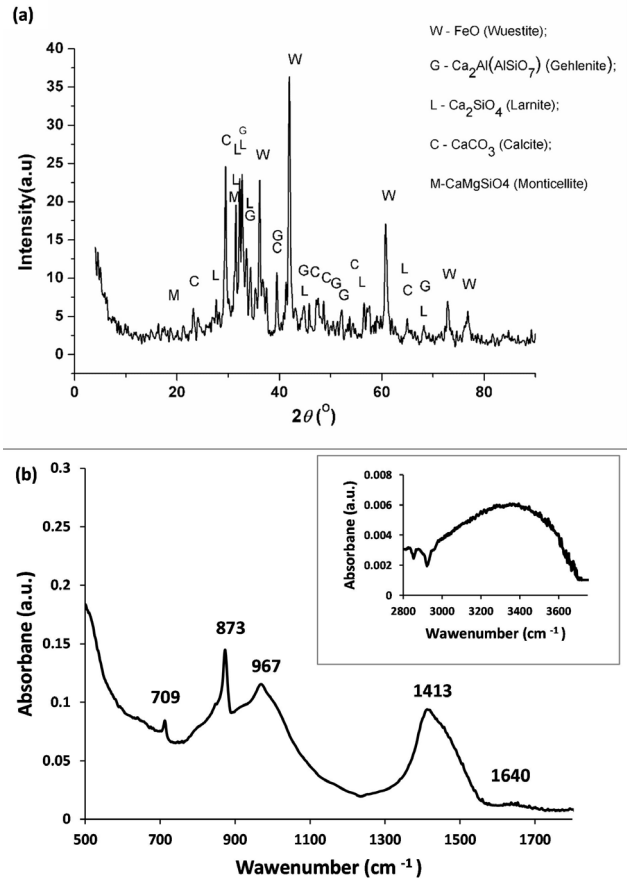

Fig. 2 X-ray difractogram (a) and FTIR spectra (b) of AA slag

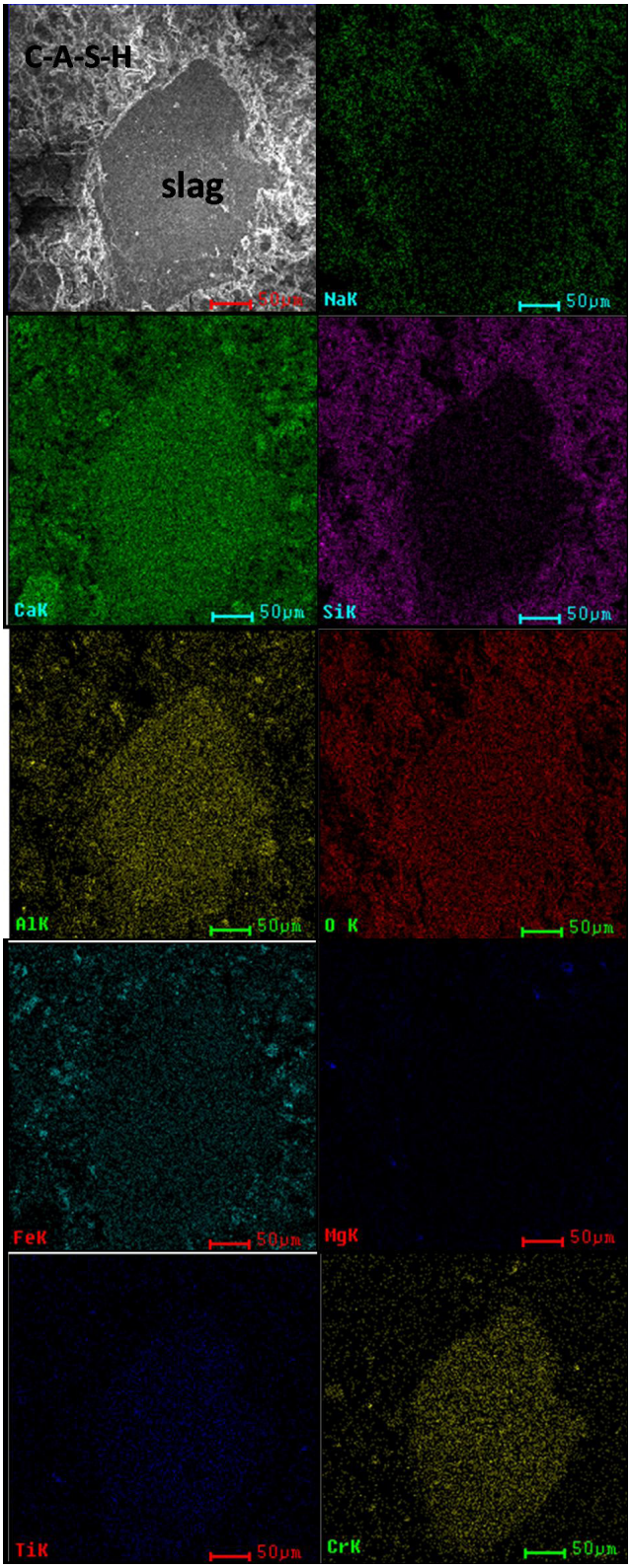

Fig. 3 SEM micrographs of the cross-section of AA slag and appropriate EDS composite maps of elemental distribution

be explained by the capability of C-A-S-H gel to incorporate (immobilize) Cr. Namely, during the process of alkaline activation of slag, chromium was dissolved to a certain extent along with other constituents of slag and become available for incorporation into the C-A-S-H structure [23].

3.2 Effect of contact time and temperature

The influence of contact time (Fig. 3) showed that the Removal Efficiency order is $Cu^{2+} > Cd^{2+} > Zn^{2+}$. The achieved Removal Efficiency of Cu^{2+}, Cd^{2+} and Zn^{2+} after 35 min at 20 °C was 54.93 %, 42 87 % and 35.86 %, respectively. Moreover, the majority of metal ions were removed from solution in the first 20 min of adsorption test which indicates that sorption of metal ions reaches equilibrium within this time. In a case of multicomponent aquatic solution, the competition of metal ions to adsorb on a specific active site of sorbent occurs. The different Removal Efficiency of metal ions is attributed to different electronegativity [24] and hydrated ionic radii of cations [25]. The metal with the highest electronegativity will be adsorbed first, and when the active sites on the sorbent are saturated with this metal, the metal with the lower electronegativity will be adsorbed [24]. This can be explained by the highest tendency of this metal ion to react with the potential adsorption sites in comparison to the ions with lower electronegativity. Thus the removal metal order ($Cu^{2+} > Cd^{2+} > Zn^{2+}$) is in agreement with the order of electronegativity of metals (Cu(1.9) > Cd(1.7) > Zn(1.6)). This order of metal adsorption on AA slag also lays in a difference in hydrated ionic radii of cations. The metal with lowest hydrated ionic radii will be adsorbed first due to faster diffusion to potential adsorption site of sorbent in a comparison to ions with higher hydrated ionic radii [25]. Thus the obtained removal metal order is also in accordance with the order of hydrated ionic radii (Cu(4.2 Å) > Cd(4.26 Å) > Zn(4.3 Å)). Since Cu are characterized by the highest electronegativity and lowest hydrated ionic radii it showed the highest affinity of Cu towards the adsorbent. Similar results for a sorption competition of these metal ions onto different adsorbent were reported earlier [26].

The efficiency of metals removal was greatly enhanced by the increase of temperature (Fig. 4) without changing the removal efficiency order. This is attributed to the enhanced mobility of metal ions on the AA slag with a rise of temperature [27]. Obtained Removal Efficiency for Cu^{2+}, Cd^{2+} and Zn^{2+} ions at 35 °C was 71.48 %, 52.5 % and 47.99 %, respectively while at 45 °C obtained Removal Efficiency was 81.98 %, 61.02 % and 51.6 %. The enhancing of adsorption of Cu^{2+}, Cd^{2+} and Zn^{2+} onto AA slag with the increase of temperature indicates the endothermic character of adsorption process.

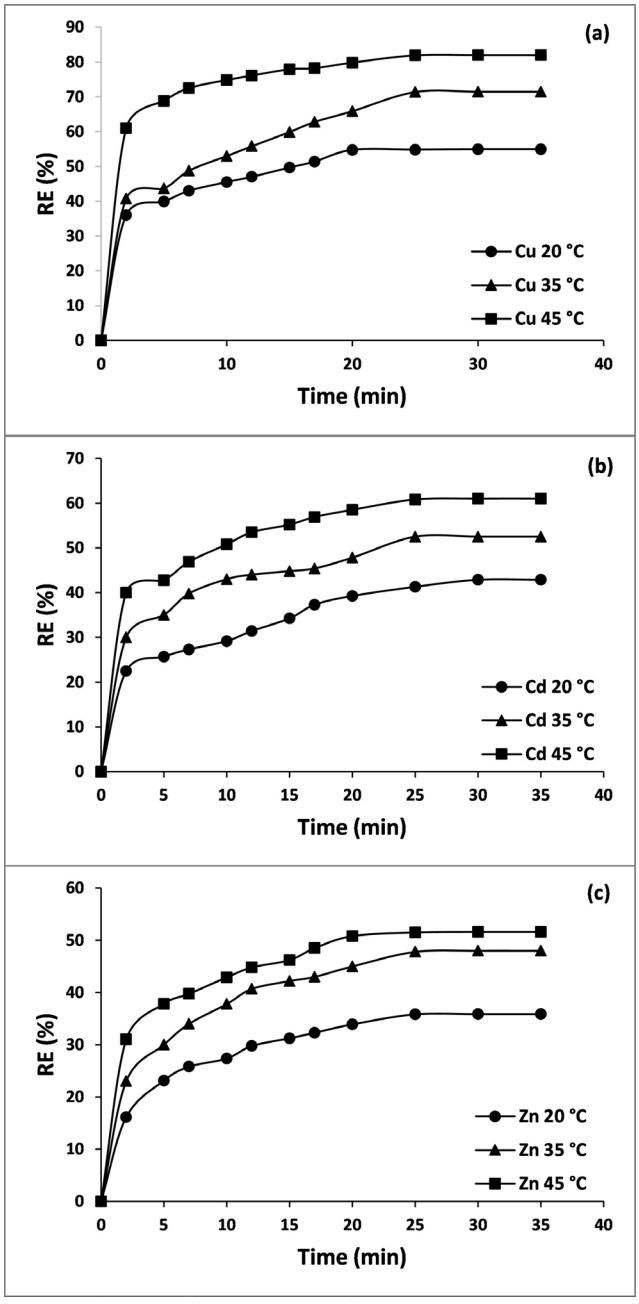

Fig. 4 Removal Efficiency of Cu^{2+}, Cd^{2+} and Zn^{2+} from aquatic solution in as function of contact time at different temperatures

3.3 Adsorption kinetics

The kinetics of metal ions adsorption onto Alkali Activated slag was studied using the pseudo-first-order and pseudo-second-order kinetics model which integrated forms are expressed by Eqs. (3) and (4), respectively:

$$\log\left(q_e - q_t\right) = \log q_e - \left(\frac{k_1}{2.303}\right)t \tag{3}$$

$$t\frac{t}{q_t} = \frac{t}{q_e} + \frac{1}{k_2 q_e^2}. \tag{4}$$

The rate constant of the pseudo first-order sorption (k_1) and the amount of metal ions adsorbed on Alkali Activated slag at equilibrium (q_e) can be calculated from the slope and intercept of straight line plots log ($q_e - q_t$) versus t. The amount of metal ions adsorbed on sorbent at any given time is denoted as q_t. The values of the rate constant of the pseudo second-order sorption (k_2) and q_e can be calculated from the intercept of and slope of the plot of t/q_t versus time. The results of kinetics analysis are given in Table 2 and Fig. 5 and Fig. 6. The values of regression coefficients R^2 and calculated equilibrium concentrations q_e were used in order to estimate the validity of applied kinetic models. It is evident that adsorption of metal ions onto Alkali Activated slag follows the pseudo-second-order kinetics models. This is due to the fact that for this model, higher values of R^2 (greater than 0.98) were achieved as well as good agreement between calculated and experimental values for q_e. This also indicate that adsorption of Cu^{2+}, Cd^{2+}, Zn^{2+} onto AA slag is dominated by the adsorption onto

Table 2 Kinetics parameters for Cu^{2+}, Cd^{2+}, Zn^{2+} adsorption onto AA slag obtained using pseudo second-order kinetic models at different temperatures

Pseudo-first-order kinetic model					
Metal ion	T (°C)	$q_{e,exp}$ (mg g^{-1})	$q_{e,cal}$ (mg g^{-1})	k_1 (min^{-1})	R^2
Cu^{2+}	20	108.17	137.06	0.17	0.8731
	35	129.96	178.5	0.11	0.9470
	45	94.38	204.95	0.15	0.8957
Cd^{2+}	20	86.72	103.22	0.10	0.8961
	35	85.37	131.15	0.12	0.9227
	45	100.00	152.00	0.14	0.954
Zn^{2+}	20	71.20	85.55	0.13	0.9761
	35	93.66	119.50	0.12	0.975
	45	102.56	128.75	0.17	0.9082
Pseudo-second-order kinetic model					
Metal ion	T (°C)	$q_{e,exp}$ (mg g^{-1})	$q_{e,cal}$ (mg g^{-1})	$k_2 \times 10^{-3}$ (g mg^{-1} min^{-1})	R^2
Cu^{2+}	20	144.93	137.05	3.56	0.9944
	35	175.44	167.75	3.61	0.9949
	45	208.33	204.75	4.81	0.9989
Cd^{2+}	20	109.89	103.23	2.99	0.9834
	35	136.99	131.25	3.21	0.99
	45	158.73	152.50	3.58	0.9954
Zn^{2+}	20	96.15	85.55	2.89	0.9849
	35	126.58 .21	119.50	3.06	0.9900
	45	125.00	128.75	3.26	0.9953

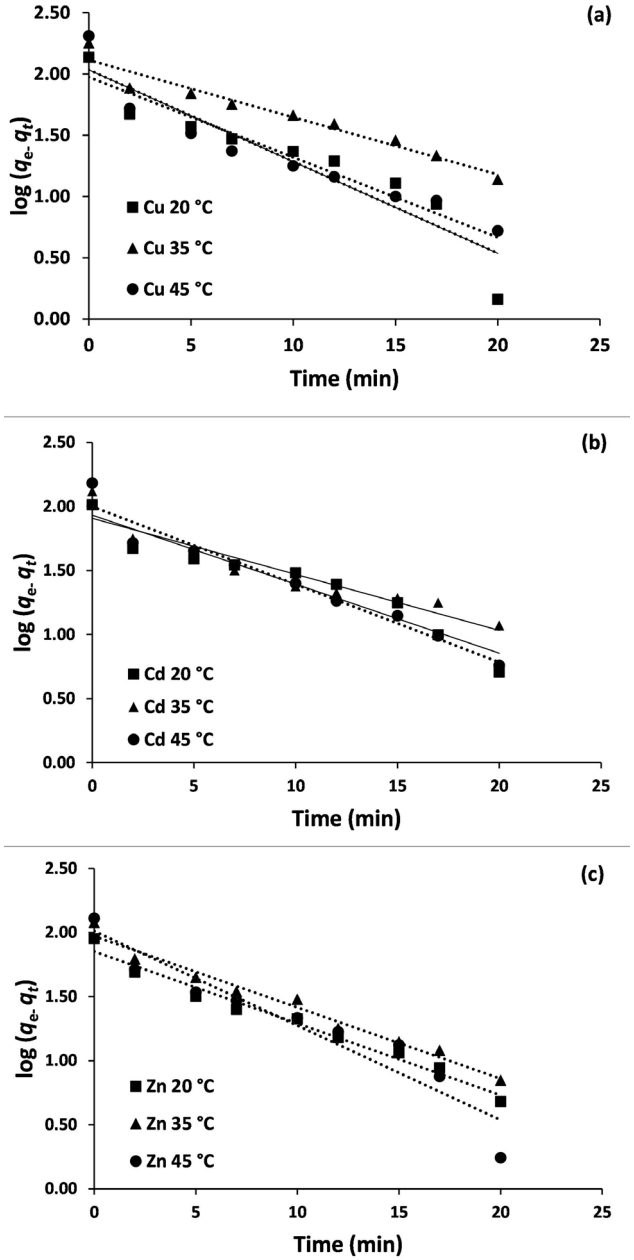

Fig. 5 The pseudofirst-order kinetics plots for the adsorption of Cu^{2+}, Cd^{2+}, Zn^{2+} onto Alkali Activated slag at different temperatures

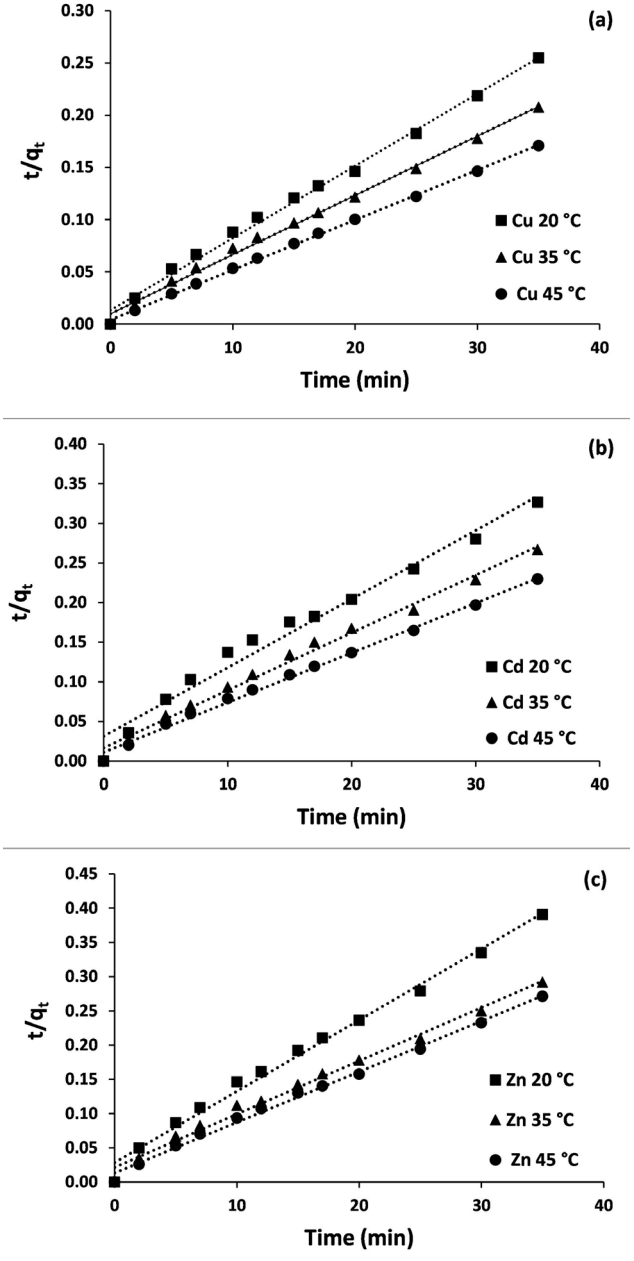

Fig. 6 The pseudo second-order kinetics plots for the adsorption of Cu^{2+}, Cd^{2+} and Zn^{2+} onto Alkali Activated slag at different temperatures

active site [28] which is in agreement with a previous finding that adsorption of heavy metals on the AA slag occurs onto silanol active groups (Si-OH) groups [29].

The value of k_2 increases with the increase of temperature, which favors the adsorption of Cu^{2+}, Cd^{2+}, Zn^{2+} onto AA slag due to the enhanced mobility of heavy metal ions [27]. Moreover, the values of k_2 obtained in this study follow the order $k_2(Cu^{2+}) > k_2(Cd^{2+}) > k_2(Zn^{2+})$ at all investigated temperatures.

3.4 Adsorption isotherms

Adsorption isotherm study was evaluated using the Langmuir (Eq. (5)) and Freundlich (Eq. (6)) isotherm models:

$$\frac{C_e}{q_e} = \frac{C_e}{Q_0} + \frac{1}{Q_0 K_L} \tag{5}$$

$$\log(q_e) = \log(K_F) + \frac{1}{n}\log(C_e), \tag{6}$$

where C_e is equilibrium concentration of metal ions. Linearized plots for Cu^{2+}, Cd^{2+}, Zn^{2+} onto AA slag obtained from the Langmuir and Freundlich models are given in Fig. 7 and Fig. 8 respectively. The slope and intercept of plots C_e/q_e gives Langmuir parameters, maximum adsorption capacity (Q_0) and Langmuir adsorption constant related to the adsorption energy (K_L). When Freundlich isotherm model is applied, values of Freundlich constant related to the adsorption capacity (K_F) and constant related to the adsorption intensity of the adsorbent ($1/n$) can be determined from the intercept and slope of $\log(q_e)$ vs $\log(C_e)$ plots, respectively. All of the Langmuir and Freundlich isotherm parameters are listed in Table 3.

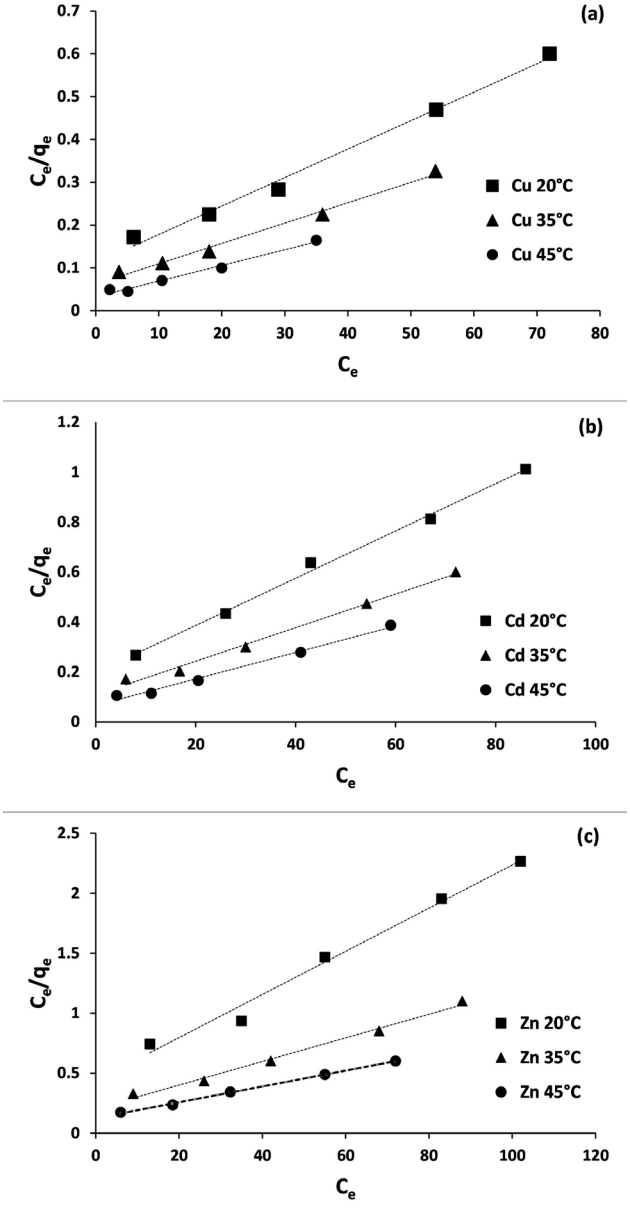

Fig. 7 Langmuir isotherms for the adsorption of Cu^{2+}, Cd^{2+} and Zn^{2+} onto AA slag

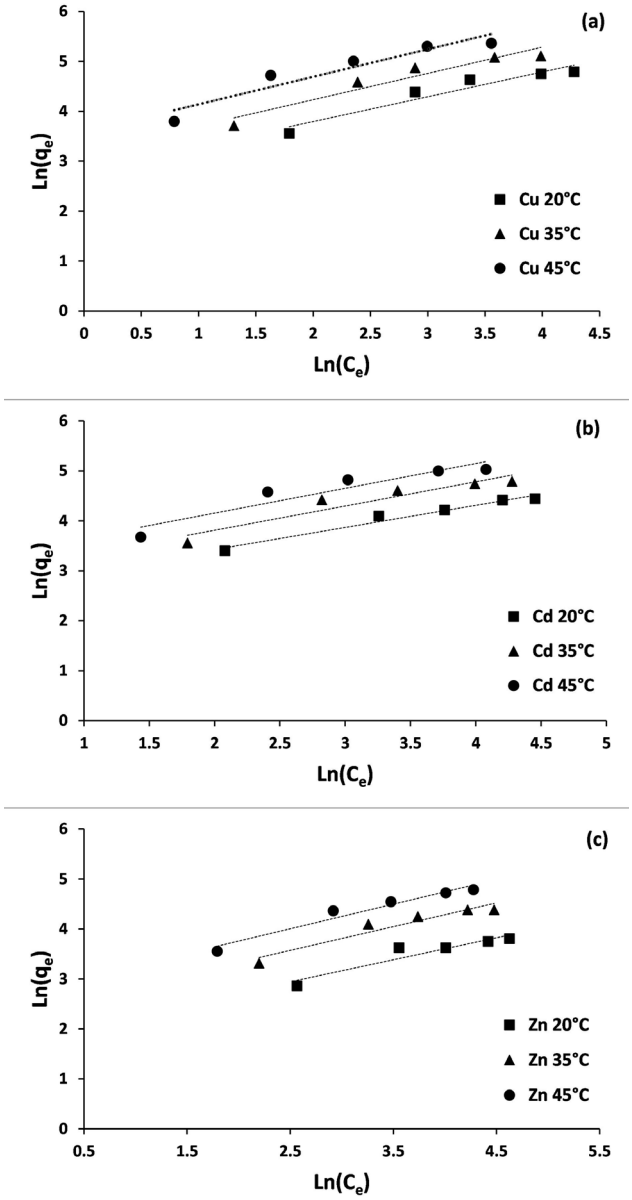

Fig. 8 Freundlich isotherms for the adsorption Cu^{2+}, Cd^{2+} and Zn^{2+} onto AA slag

Analysis of experimental data (Table 3) has shown that high values of R^2 ($R^2 > 0.98$) was achieved when Langmuir models was applied which indicates that adsorption Cu^{2+}, Cd^{2+}, and Zn^{2+} on AA slag occurs on a homogenous surface of AA slag covered by a monolayer of the adsorbate.

The adsorption capacity (Q_0) increased with a corresponding rise in temperature and changed in the order of $Q_0(Cu^{2+}) > Q_0(Cd^{2+}) > Q_0(Zn^{2+})$ at all investigated temperatures.

3.5 Adsorption mechanism

Mechanism of adsorption of Cu^{2+} onto AA slag was investigated using the intraparticle diffusion model [29].

Table 3 Isotherms parameters for Cu^2, $Cd^{2+}$and Zn^{2+} adsorption onto AA slag

Metal ion	T (°C)	Q_0 (mg g^{-1})	K_L (L mg^{-1})	R^2
		Langmuir isotherm model		
Cu^{2+}	20	151.51	0.061	0.9923
	35	212.76	0.083	0.9910
	45	270.27	0.115	0.9832
Cd^{2+}	20	105.26	0.042	0.9955
	35	151.51	0.066	0.9923
	45	188.68	0.080	0.9893
Zn^{2+}	20	84.74	0.033	0.9851
	35	101.01	0.051	0.9908
	45	178.57	0.068	0.9983
		Freundlich isotherm model		
Metal ion	T (°C)	K_F $\left(\text{mg g}^{-1}\left(\text{L mg}^{-1}\right)^{n^{-1}}\right)$	n	R^2
Cu^{2+}	20	16.50	2.021	0.9184
	35	23.99	1.901	0.9217
	45	36.20	1.820	0.9008
Cd^{2+}	20	14.12	2.473	0.9181
	35	17.22	2.075	0.9033
	45	23.60	2.011	0.8886
Zn^{2+}	20	6.31	2.273	0.8881
	35	10.86	2.112	0.9199
	45	16.07	2.024	0.9523

The three main steps occur during the adsorption process in a solid-liquid system: film diffusion, intraparticle diffusion and adsorption of metal ions onto the active groups of adsorbents. The overall rate of metal ions adsorption is determined by the rate of the lowest step.

Since the third step is very fast, the overall rate of adsorption is controlled by the film or intraparticle diffusion. Intraparticle diffusion model (Eq. (7)) [30] is often used to analyze the effects of intraparticle and film diffusion of metal ions onto adsorbents through analysis of intraparticle diffusion rate k_i and constant C.

$$q_t = k_i t^{0.5} + C \tag{7}$$

The slope and intercept of plots q_t against $t^{0.5}$ (Fig. 9) enables determination of k_i and C, for Cu^{2+}, Cd^{2+} and Zn^{2+} adsorption onto AA slag at various temperatures. The obtained plots are multilinear indicating that multiple mechanisms control the adsorption process. The first, second and third line segments are attributed to film diffusion, intraparticle diffusion and equilibrium stage, respectively. The results indicate that adsorption of metal ions onto AA slag was not solely governed by intraparticle diffusion but

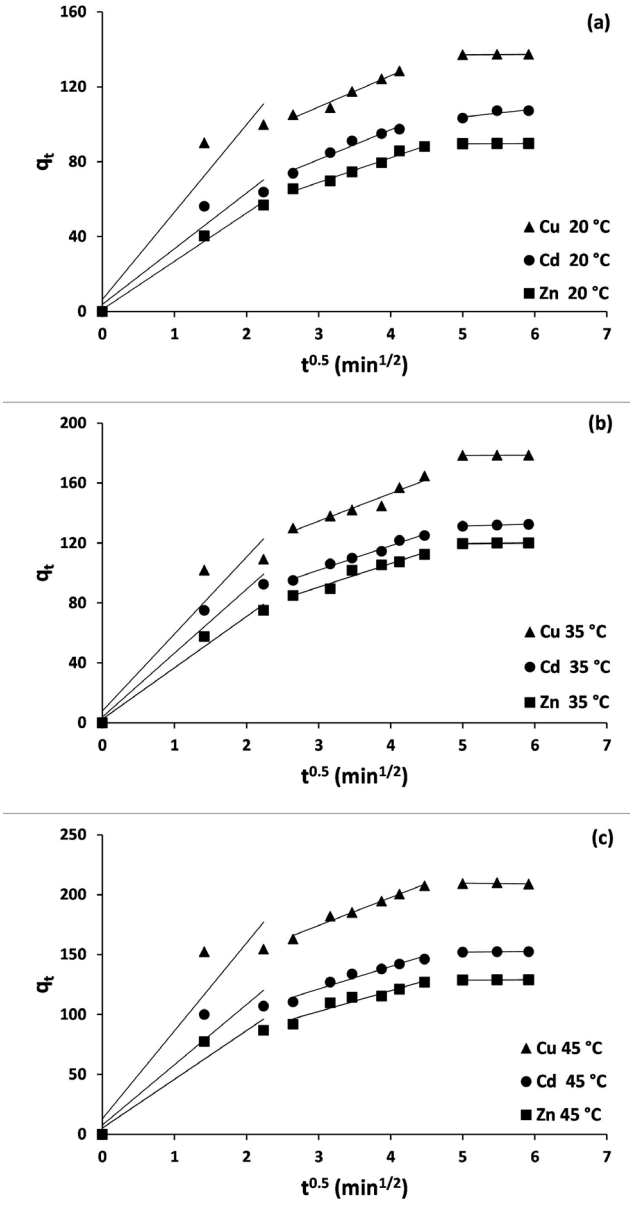

Fig. 9 Intraparticle diffusion plots for Cu^{2+}, Cd^{2+} and Zn^{2+} adsorption onto AA slag at different temperatures

by film diffusion as well since the second segments of plots q_t vs $t^{0.5}$ (Fig. 9) exhibit non-zero intercepts [31]. It means that rate controlling steps are not only intraparticle diffusion but also the film diffusion. The results of analysis of mechanism of adsorption (Table 4) indicate the decrease of intraparticle diffusion and increased film diffusion effect with the rise of temperature since decrease of k_i and increase of C values with the rise of temperature were observed [27].

The higher values of C are ascribed to the higher resistance of liquid boundary layer to mass transfer of metal ions which slows down the film diffusion [32]. Thus, the role of film diffusion as a rate limiting step becomes more important at higher temperatures [33].

Table 4 Adsorption mechanism data of Cu^{2+}, Cd^{2+} and Zn^{2+} adsorption on AA slag

Ion	T (°C)	k_i (mg g^{-1} min$^{-0.5}$)	C	R^2
Cu^{2+}	20	15.28	65.79	0.9884
	35	13.08	107.97	0.9639
	45	11.48	149.15	0.9623
Cd^{2+}	20	13.68	34.87	0.9622
	35	12.75	64.98	0.9858
	45	11.76	93.07	0.9817
Zn^{2+}	20	13.14	26.86	0.9835
	35	12.64	58.12	0.9620
	45	11.72	72.59	0.9573

Table 5 Thermodynamic parameters of Cu^{2+}, Cd^{2+} and Zn^{2+} adsorption and AA slag

Ion	T (°C)	K_d	$-\Delta G°$ (KJ mol^{-1})	$\Delta H°$ (KJ mol^{-1})	$\Delta S°$ (J mol^{-1} K^{-1})
Cu^{2+}	20	3.03	2.70	36.35	133.12
	35	5.81	4.50		
	45	9.94	6.07		
Cd^{2+}	20	1.76	1.37	24.32	87.62
	35	2.76	2.60		
	45	3.88	3.58		
Zn^{2+}	20	1.52	1.02	17.42	62.85
	35	2.20	2.02		
	45	2.65	2.58		

3.6 Thermodynamic study

The following thermodynamic equations were used in the thermodynamic analysis of Cu^{2+}, Cd^{2+} and Zn^{2+} adsorption onto AA slag:

$$\Delta G° = \Delta H° - T\Delta S° \tag{8}$$

$$\Delta G° = -RT \ln K_d \tag{9}$$

$$\ln K_d = \frac{\Delta S°}{R} - \frac{\Delta H°}{RT} \tag{10}$$

$$K_d = \frac{(C_0 - C_e) \times V}{C_e \times m}. \tag{11}$$

The values of thermodynamic parameters, standard free energy $\Delta G°$, enthalpy $\Delta H°$, entropy $\Delta S°$ and equilibrium distribution coefficient K_d are given in Table 5. The Values of $\Delta H°$ and $\Delta S°$ are calculated from the slope ($\Delta H°/R$) and intercept ($\Delta S°/R$) of the straight-line plots ln K_d vs 1000/T (Fig. 10). The results of thermodynamic analysis indicate endothermic character of adsorption process of Cu^{2+}, Cd^{2+} and Zn^{2+} onto AA slag since values of $\Delta H°$ was calculated to be positive (Table 5).

Moreover the values of $\Delta H°$ give information on the type of adsorption. The values of enthalpy obtained in this study were lower than 40 kJ mol^{-1}, which indicates the weak bonds between adsorbent and adsorbate *e.g.* physisorption is involved in the adsorption process [33].

The values of K_d obtained in this study follow the order $k_d(Cu^{2+}) > k_d(Cd^{2+}) > k_d(Zn^{2+})$ at all investigated temperatures which indicate that affinity of AA slag towards the investigated metal ions follow the order of $Cu^{2+} > Cd^{2+} > Zn^{2+}$ ions. Negative values of free energy ($\Delta G°$) indicate that Cu^{2+}, Cd^{2+} and Zn^{2+} adsorption onto AA slag occurs spontaneously at all investigated temperatures

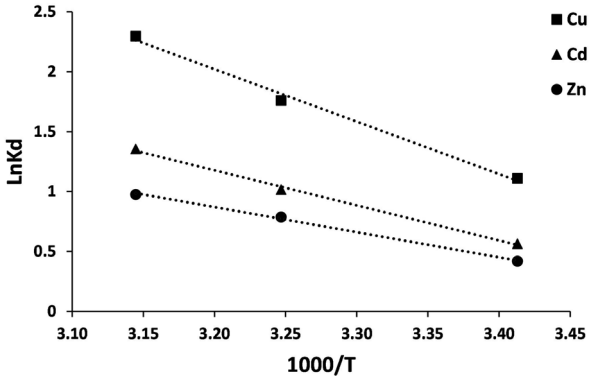

Fig. 10 Plots ln K_d vs 1000/T

and the decrease of $\Delta G°$ with the rise of temperature indicate that adsorption of metal ions onto AA slag sorbent is more favorable at higher temperatures. Moreover, the negative values of $\Delta G°$ follow the order of $Cu^{2+} > Cd^{2+} > Zn^{2+}$ indicating that highest affinity of AA slag towards Cu^{2+} ions at all investigated temperatures.

4 Conclusion

In this paper EAF slag was used as a precursor for synthesis of AA slag instead of frequently used Granulated Blast Furnace Slag. AA slag was characterized by XRD, FTIR and SEM/EDS which confirmed the presence of C-A-S-H gel in AA slag sample. Such prepared AA slag was used for the investigation of Cu^{2+}, Cd^{2+} and Zn^{2+} removal from aquatic solution containing all three ions. The results of adsorbtion tests have shown that AA slag can be used as an effective adsorbent for simultaneous removal of Cu^{2+}, Cd^{2+} and Zn^{2+} from aquatic solution containing all three metal ions. The Removal Efficiency of heavy metals decrease in the order of Cu^{2+} (54.93 %) > Cd^{2+} (42.87 %) > Zn^{2+} (35.86 %) at 20 °C. The rise of temperature enhances the adsorption process.

Adsorption of these metal ions onto AA slag follow the second-order kinetic model and both intraparticle and film diffusion control the adsorption process at all investigated temperatures. Langmuir model best describes the metal adsorption onto AA slag Thermodynamic analysis indicated that adsorption process is endothermic and more feasible at higher temperatures. The AA slag sorbent displayed the highest affinity towards the Cu^{2+} ions.

Acknowledgement

The authors would like to thank dr. Smilja Marković and dr. Ljiljana Veselinović from the Institute of Technical Sciences of SASA, Belgrade, Serbia, for technical support in FTIR, XRPD and particle size investigations. The authors acknowledge Prof. dr Velimir Radmilović from the Serbian Academy of Sciences and Arts for the support in a microstructural investigation.

References

[1] Herawati, N., Suzuki, S., Hayashi, K., Rivai, I. F., Koyama, H. "Cadmium, Copper, and Zinc Levels in Rice and Soil of Japan, Indonesia, and China by Soil Type", Bulletin of Environmental Contamination and Toxicology, 64, pp. 33–39, 2000. https://doi.org/10.1007/s001289910006

[2] Izah, S. C., Chakrabarty, N., Srivastav, A. L. "A Review on Heavy Metal Concentration in Potable Water Sources in Nigeria: Human Health Effects and Mitigating Measures", Exposure and Health, 8, pp. 285–304, 2016. https://doi.org/10.1007/s12403-016-0195-9

[3] Mo, J., Yang, Q., Zhang, N., Zhang, W., Zheng, Y., Zhang, Z. "A review on agro-industrial waste (AIW) derived adsorbents for water and wastewater treatment", Journal of Environmental Management, 227, pp. 395–405, 2018. https://doi.org/10.1016/j.jenvman.2018.08.069

[4] Ahmed, M. J. K., Ahmaruzzaman, M. "A review on potential usage of industrial waste materials for binding heavy metal ions from aqueous solutions", Journal of Water Process Engineering, 10, pp. 39–47, 2016. https://doi.org/10.1016/j.jwpe.2016.01.014

[5] Shyam, R., Puri, J. K., Kaur, H., Kapila. A. "Single and binary adsorption of heavy metals on fly ash samples from aqueous solution", Journal of Molecular Liquids, 178, pp. 31–36, 2013. https://doi.org/10.1016/j.molliq.2012.10.031

[6] Bhatnagar, A., Vilar,V. J. P., Cidália M. S. Botelho, C. M. S., Boaventura, R. A. R "A review of the use of red mud as adsorbent for the removal of toxic pollutants from water and wastewater", Environmental Technology, 32(3), pp. 231–249, 2011. https://doi.org/10.1080/09593330.2011.560615

[7] Wang, Z., Huang, G., An, C., Chen, L., Liu, J. "Removal of copper, zinc and cadmium ions through adsorption on water-quenched blast furnace slag", Desalination and Water Treatment, 57(47), pp. 22493–22506, 2016. https://doi.org/10.1080/19443994.2015.1135084

[8] Liu, S.-Y., Gao, J., Yang, Y.-J., Yang, Y.-C., Ye, Z.-X. "Adsorption intrinsic kinetics and isotherms of lead ions on steel slag", Journal of Hazardous Materials, 173(1–3), pp. 558–562, 2010. https://doi.org/10.1016/j.jhazmat.2009.08.122

[9] Deng, X., Qi, L., Zhang, Y. "Experimental Study on Adsorption of Hexavalent Chromium with Microwave-Assisted Alkali Modified Fly Ash", Water Air & Soil Pollution, 229, Article number: 18, 2018. https://doi.org/10.1007/s11270-017-3679-8

[10] Xiyili, H., Çetintaş, S., Bingöl, D. "Removal of some heavy metals onto mechanically activated fly ash: Modeling approach for optimization, isotherms, kinetics and thermodynamics", Process Safety and Environmental Protection, 109, pp. 288–300, 2017. https://doi.org/10.1016/j.psep.2017.04.012

[11] Pizarro, J., Castillo, X., Jara, S., Ortiz, Q., Navarro, P., Cid, H., Rioseco, H., Barros, D., Belzile, N. "Adsorption of Cu^{2+} on coal fly ash modified with functionalized mesoporous silica", Fuel, 156, pp. 96–102, 2015. https://doi.org/10.1016/j.fuel.2015.04.030

[12] He, K., Chen, Y., Tang, Z., Hu. J. "Removal of heavy metal ions from aqueous solution by zeolite synthesized from fly ash", Environmental Science and Pollution Research, 23, pp. 2778–2788, 2016. https://doi.org/10.1007/s11356-015-5422-6

[13] Genç, H., Tjell, J. C., McConchie, D., Schuiling, O. "Adsorption of arsenate from water using neutralized red mud", Journal of Colloid and Interface Science, 264(2), pp. 327–334, 2003. https://doi.org/10.1016/S0021-9797(03)00447-8

[14] Khan, T. A., Chaudhry, S. A., Ali, I. "Equilibrium uptake, isotherm and kinetic studies of Cd(II) adsorption onto iron oxide activated red mud from aqueous solution", Journal of Molecular Liquids, 202, pp. 165–175, 2015. https://doi.org/10.1016/j.molliq.2014.12.021

[15] Sahu, M. K., Mandal, S., Dash, S. S., Badhai, P., Patel, R. K. "Removal of Pb(II) from aqueous solution by acid activated red mud", Journal of Environmental Chemical Engineering, 1(4), pp. 1315–1324, 2013. https://doi.org/10.1016/j.jece.2013.09.027

[16] Zhao, Y., Chen, H., Yan, Q. "Enhanced phosphate removal during the simultaneous adsorption of phosphate and Ni^{2+} from electroless nickel wastewater by calcium silicate hydrate (CSH)", Environmental Technology & Innovation, 8, pp. 141–149, 2017. https://doi.org/10.1016/j.eti.2017.01.002

[17] Coleman, N. J., Brassington, D. S., Raza, A., Lee, W. E. "Calcium Silicate Sorbent from Secondary Waste Ash: Heavy Metals-Removal from Acidic Solutions", Environmental Technology, 27(10), pp. 1089–1099, 2006. https://doi.org/10.1080/09593332708618724

[18] Pacheco-Torgal, F., Castro-Gomes, J., Jalali, S. "Alkali-activated binders: A review: Part 1. Historical background, terminology, reaction mechanisms and hydration products", Construction and Building Materials, 22(7), pp. 1305–1314, 2008. https://doi.org/10.1016/j.conbuildmat.2007.10.015

[19] Nikolić, I., Karanović, l., Janković Častvan, I., Radmilović, V., Mentus, S., Radmilović, V. "Improved compressive strength of alkali activated slag upon heating", Matererial Letters, 133, pp. 251–254, 2014.
https://doi.org/10.1016/j.matlet.2014.07.021

[20] Zhang, N., Li, H., Zhao, Y., Liu, X. "Hydration characteristics and environmental friendly performance of a cementitious material composed of calcium silicate slag", Journal of Hazardous Materials, 306, pp. 67–76, 2016.
https://doi.org/10.1016/j.jhazmat.2015.11.055

[21] Puertas, F., Palacios, M., Manzano, H., Dolado, J. S., Rico, A., Rodríguez, J. "A model for the C-A-S-H gel formed in alkali-activated slag cements", Journal of the European Ceramic Society, 31(12), pp. 2043–2056, 2011.
https://doi.org/10.1016/j.jeurceramsoc.2011.04.036

[22] Yip, C. K., Lukey, G. C., van Deventer, J. S. J. "The coexistence of geopolymeric gel and calcium silicate hydrate at the early stage of alkaline activation", Cement and Concrete Research, 35(9), pp. 1688–1697, 2005.
https://doi.org/10.1016/j.cemconres.2004.10.042

[23] Huang, X., Huang, T., Li, S., Muhammad, F., Xu, G., Zhao, Z., Yu, L., Yan, Y., Li, D., Jiao, B. "Immobilization of chromite ore processing residue with alkali-activated blast furnace slag-based geopolymer", Ceramics International, 42(8), pp. 9538–9549, 2016.
https://doi.org/10.1016/j.ceramint.2016.03.033

[24] Üçer, A., Uyanik, A., Aygün, S. F. "Adsorption of Cu(II), Cd(II), Zn(II), Mn(II) and Fe(III) ions by tannic acid immobilised activated carbon", Separation and Purification Technology, 47(3), pp. 113–118, 2006.
https://doi.org/10.1016/j.seppur.2005.06.012

[25] Sheela, T., Nayaka, Y. A., Viswanatha, R., Basavanna, S., Venkatesha, T. G. "Kinetics and thermodynamics studies on the adsorption of Zn(II), Cd(II) and Hg(II) from aqueous solution using zinc oxide nanoparticles", Powder Technology, 217, pp. 163–170, 2012.
https://doi.org/10.1016/j.powtec.2011.10.023

[26] Nguyen, T. C., Loganathan, P., Nguyen, T. V., Vigneswaran, S., Kandasamy, J., Naidu, R. "Simultaneous adsorption of Cd, Cr, Cu, Pb, and Zn by an iron-coated, Australian zeolite in batch and fixed-bed column studies", Chemical Engineering Journal, 270, pp. 393–404, 2015.
https://doi.org/10.1016/j.cej.2015.02.047

[27] Song, G., Zhu, X., Chen, R., Liao, Q., Ding, Y-D., Chen, L. "An investigation of CO_2 adsorption kinetics on porous magnesium oxide", Chemical Engineering Journal, 283, pp. 175–183. 2016.
https://doi.org/10.1016/j.cej.2015.07.055

[28] Wang, J., Guo, X. "Adsorption kinetic models: Physical meanings, applications, and solving methods", Journal of Hazardous Materials 390, Article number: 122156, 2020.
https://doi.org/10.1016/j.jhazmat.2020.122156

[29] Nikolić, I., Marković, S., Veselinović, Lj., Radmilović, V. V., Janković-Častvan, I., Radmilović, V. R. "Enhanced sorption of of Cu^{2+} from sulfate solutions onto modified electric arc furnace slag", Materials Letters, 235, pp. 184–188, 2019.
https://doi.org/10.1016/j.matlet.2018.10.027

[30] Weber, W. J., Morris, J. C. "Kinetics of Adsorption on Carbon from Solution", Journal of the Sanitary Engineering Division, 89(2), pp. 31–60, 1963.

[31] Kumar, D., Gaur, J. P. "Chemical reaction- and particle diffusion-based kinetic modeling of metal biosorption by a *Phormidium* sp.-dominated cyanobacterial mat", Bioresource Technology, 102(2), pp. 633–640, 2011.
https://doi.org/10.1016/j.biortech.2010.08.014

[32] Cigu, T. A., Vasiliu, S, Racovita, S., Lionte, C., Sunel, V., Popa, M., Cheptea, C. "Adsorption and release studies of new cephalosporin from chitosan-*g*-poly(glycidyl methacrylate) microparticles", European Polymer Journal, 82, pp. 132–152, 2016.
https://doi.org/10.1016/j.eurpolymj.2016.07.011

[33] Gusain, D., Srivastava, V., Sharma, Y. C. "Kinetic and thermodynamic studies on the removal of Cu(II) ions from aqueous solutions by adsorption on modified sand", Journal of Industrial Engineering Chemistry, 20(3), pp. 841–847. 2014.
https://doi.org/10.1016/j.jiec.2013.06.014